



Article

Effects of Post-Synthesis Activation and Relative Humidity on Adsorption Performance of ZIF-8 for Capturing Toluene from a Gas Phase in a Continuous Mode

Saeed Jafari ¹ , Farshid Ghorbani-Shahna ^{1,*}, Abdulrahman Bahrami ² and Hossein Kazemian ³ 

¹ Center of Excellence for Occupational Health and Research Center for Health Science, School of Public Health, Hamadan University of Medical Sciences, Hamadan 6517838736, Iran; Jafari4514@gmail.com

² Occupational Health and Safety Research Center, School of Public Health, Hamadan University of Medical Sciences, Hamadan 6517838736, Iran; bahrami@umsha.ac.ir

³ College of Science and Management, University of Northern British Columbia, Prince George, BC V2N 4Z9, Canada; hossein.kazemian@unbc.ca

* Correspondence: fghorbani@umsha.ac.ir; Tel.: +98-81-3838-0025

Received: 20 December 2017; Accepted: 11 February 2018; Published: 22 February 2018

Abstract: Zeolitic imidazolate framework-8 (ZIF-8) was used as an adsorbent for the removal of toluene in its gas phase at different relative humidity (RH). High-purity ZIF-8 with an average particle size of 0.64 μm synthesized from an aqueous solution at room temperature, and then characterized by X-ray diffraction (XRD), fourier transform infrared (FT-IR) and scanning electron microscopy (SEM) techniques. Dynamic adsorption (continuous mode) experiments of toluene on ZIF-8 were studied using breakthrough curves. The effects of thermal pretreatment (activation) under dry air and N_2 atmospheres on the adsorbent performances was studied. ZIF-8 activated at 300 $^\circ\text{C}$ for 3 h under dry air showed the highest adsorption capacity of 562.17 $\text{mg}\cdot\text{g}^{-1}$. Furthermore, it was observed that the adsorption of toluene on ZIF-8 was significantly decreased at 80% RH. The experimental data of dynamic adsorption well fitted into the Thomas and Yan mathematical models.

Keywords: zeolitic imidazolate framework-8; ZIF-8; metal organic framework; toluene; adsorption; relative humidity (RH)

1. Introduction

Volatile organic compounds (VOCs) are a wide array of hydrocarbon-based gases and vapors that are known as one of the major contributors to air pollution. VOCs can be found in various industrial exhausts including, but not limited to, transportation, chemical industries, petrochemical plants, and petroleum refineries [1]. VOCs' high vapor pressure, low boiling point, and strong reactivity contribute to their photochemical reaction in the atmosphere [2]. Many negative impacts of VOCs on human health and the environment, such as their contribution to the depletion of the ozone layer, photochemical ozone formation in the tropospheric layer, global greenhouse effect, and contribution to the formation of fine particulate matter ($\text{PM}_{2.5}$), have been reported [3,4]. Some VOCs are known carcinogenic, mutagenic, and neurotoxic chemicals [5].

Due to the negative effects of VOCs on humans and the environment, and the fact that their concentration in the atmosphere is increasing (e.g., as a result of industrialization), environmental regulations aim to control and decrease the emission of VOCs into the environment. The Goteborg Protocol recommendation is to decrease the world's VOC emission by 50% by 2020 compared to the

base year of 2000 [4,6]. Accordingly, in recent years, great efforts have been made to develop new and more efficient techniques for VOC abatement from emission sources.

A wide array of physicochemical technologies, such as thermal and catalytic oxidation, photocatalytic oxidation [7], biological degradation [8,9], condensation, adsorption, and absorption [3], have been used for capturing VOCs from industrial exhausts [10]. In comparison to other air pollution control technologies, adsorption-based technologies are being considered as simple, capable to manage multicomponent pollutants, efficient and cost effective process that can be used for capturing and recovering VOCs at different concentrations [11,12]. While adsorption can occur at all solid-gas interfaces, however, the capacity of adsorbents to capture the adsorbate molecules depends on the different characteristics of adsorbents including specific surface area, pore size distribution [13,14], pore volume, particle size, presence of functional groups, and a preferential affinity for the target adsorbate [15].

Several categories of materials are known as efficient adsorbents for removal of different air pollutants, in which activated carbon, silica gel, alumina oxide, and several types of zeolites are the most common ones [16]. While activated carbon is widely used, however, it has several disadvantages including: inflammability risk, low thermal stability, pores blockage, and problems associated with regeneration processes [2,11,12,17]. Activated carbon is not a selective adsorbent, and we cannot control and tune its pore size because of its amorphous structure [18]. In order to overcome the problems associated with the commercially-available adsorbents (e.g., activated carbon), development of new porous materials as more efficient adsorbents is an emerging area of research with massive interest.

Metal organic frameworks (MOFs) or organic-inorganic hybrid solids, also known as porous coordination polymers (PCPs), have attracted great attention in recent years because of their unique structural chemistry including, but not limited to, high surface area, their possibility to incorporate functional groups, and tunable porosities [19,20]. MOFs can be used as adsorbents [21,22], and in catalysis [23–25], drug delivery [26], chemical sensors [27], and for different energy applications [28].

Zeolitic imidazole frameworks (ZIFs) are a subgroup of MOFs with a crystal structure similar to zeolites. In ZIF structure, a metal ion ($M = Zn^{2+}$ or Co^{2+}) replaces Si and Al tetrahedral and an imidazolate (Im) linker replaces the bridging oxygen in zeolites. The composed M-Im-M angle is $\sim 145^\circ$, which is similar to the Si-O-Si angle of zeolite crystal structure [29–32].

Different types of ZIFs are synthesized in which ZIF-8 has gained remarkable attention because of its unique properties. ZIF-8 composed of Zn (II) linked with 2-methylimidazolate bridges forming a sodalite (SOD)-like structure similar to Y and X types of zeolite structures. ZIF-8's porous structure is composed of large cavities with 1.16 nm diameters, connected through 0.34 nm pore openings [29,33,34]. ZIF-8 has high thermal and chemical stability that cannot be seen in many MOFs and other ZIFs [29,31,35]. ZIF-8 is stable in refluxing benzene, methanol, water, and aqueous sodium hydroxide for seven days at different temperatures, from 25 °C to the boiling point of each solvent [31]. The crystal structure of ZIF-8 is stable in air for 5 h at 300 °C, in argon for 5 h at 400 °C, and in N_2 at 550 °C [36,37], and under pressure [38].

For the first time, Yaghi et al. synthesized ZIF-8 in 2006 by dissolving 2-methylimidazol and zinc nitrate tetrahydrate in dimethylformamide (DMF) at 140 °C for 24 h [31]. Trapping of DMF molecules inside the ZIF-8 cavities was one of the disadvantages of Yaghi's method [32]. Since then, many other research teams synthesized ZIF-8 using different solvents with smaller kinetic diameters [32], such as methanol [39], and straight and branched aliphatic alcohols [40]. These organic solvents are toxic and expensive. Recently, a great deal of effort has been made to synthesize ZIF-8 in aqueous solution by using metal to ligand ratios of 2 ($Zn:Hmim = 2$) [32,41].

He et al. synthesized ZIF-8 from stoichiometric Zn and Hmim in the presence of ammonium hydroxide at room temperature with $Zn:Hmim:NH_3:H_2O$ molar ratio of 1:2:32:157 [32].

In this study, we synthesized ZIF-8 using an environmentally-friendly method in aqueous solution at room temperature. ZIF-8 samples were characterized using scanning electron microscopy (SEM), X-ray diffraction (XRD), and FT-IR techniques. The effect of humidity on adsorption properties of

toluene on ZIF-8 samples were studied. The effect of humidity on adsorption capacity/efficiency is an important factor for application of sorbents in real conditions. The adsorption experiments were carried out in a fixed-bed adsorption setup. Adsorption behavior of the ZIF-8 samples (as synthesized and thermally-activated) toward toluene was studied at different RH. The experimental data were fitted into the Thomas and Yan mathematical models.

2. Materials and Methods

2.1. Sample Preparation

Zinc nitrate hexahydrate [$\text{Zn}(\text{NO}_3)_2 \cdot 6\text{H}_2\text{O}$], 2-methylimidazole (Hmim, $\text{C}_4\text{H}_6\text{N}_2$), and ammonium hydroxide (NH_3 , 28–30% aqueous solution,) were purchased from Sigma-Aldrich (St. Louis, MO, USA). All chemicals were used without further purification.

Synthesis of ZIF-8 was carried out according to a procedure reported by He et al. [32]. Briefly, 1.18 g of $\text{Zn}(\text{NO}_3)_2 \cdot 6\text{H}_2\text{O}$ was dissolved in 6 mL of deionized (DI) water. Then 0.66 g of 2-methylimidazole was dissolved in 8.35 mL of ammonium hydroxide solution. The zinc solution was added slowly to the 2-methylimidazole solution under stirring. The mixture immediately converted to a milky suspension. Then stirred for another 10 min at room temperature. The milky suspension was centrifuged at 4000 rpm for 10 min and the supernatant was separated (decanted). In order to wash the synthesized ZIF-8, the product was dispersed in 60 mL DI water and centrifuged again. Washing was repeated three times. The washed product was dried at 60 °C overnight in an oven prior to conducting characterization analyses.

2.2. Characterization

Crystallinity and purity of the synthesized samples were studied using X-ray diffraction (XRD). The XRD patterns were acquired using a D8 Advance instrument (Bruker, Karlsruhe, Germany) (Cu $K\alpha$ radiation). All the XRD patterns were collected at a scan rate of 2°/min and step size of 0.02° between 5 and 40 (2 θ) degrees. Fourier transform infrared (FT-IR) spectra were examined to confirm the formation of ZIF-8 as well as to compare the effects of various condition on the samples structure. FT-IR spectra were attained using a PerkinElmer-Spectrum RXI infrared spectrometer (PerkinElmer, Waltham, MA, USA). Scanning electron microscopy (SEM) was performed to observe the morphology and determine particle sizes of the synthesized ZIF-8. SEM micrographs were obtained using a CamScan Device MV 2300 (CamScan, Kingston, ON, Canada) at an acceleration voltage of 20 kV. In order to conduct SEM tests, the samples were mounted on conductive carbon double-sided sticky tape and a thin layer of gold was coated on the samples to decrease charging effects. Mean, standard deviation, and the particle size distribution of ZIF-8 was measured manually using Photoshop software from the SEM image. The diameter of about 100 particles in the SEM image were measured to determine these parameters.

2.3. The Experimental Setup

Adsorption parameters of ZIF-8 were determined under various conditions using a fixed bed reactor. Known concentration of toluene vapor was generated by injection pure toluene (Merck, Kenilworth, NJ, USA, 99.99%) with the optimum constant flow rate into the dried and pure N_2 (99.999) as the carrier gas. The injection of toluene was performed by a syringe pump (Chymex fusion 100, Houston, TX, USA) and N_2 flow rate was controlled by mass flow controller (Alicat MC-Series, Tucson, AZ, USA). The relative humidity was generated by mixing water vapor with the carrier gas. For this purpose, a container with 20 mL distilled water was placed on a constant-temperature silicon oil bath. A PID-type thermostat (Autonics, Busan, Korea) controlled the temperature of the oil bath. In this condition, water vapor was generated with a constant rate. The adsorbent was packed into a quartz tube, with 15 cm length and 0.5 cm internal diameters, using glass wool on both sides to fix it. Toluene concentrations in the influent and effluent were measured using a gas chromatograph

equipped with a CP-Sil 5 CB capillary column and a flame ionization detector (GC-FID; Varian CP 3800, Santa Clara, CA, USA).

2.4. Measurement of Toluene Dynamic Adsorption Capacity

Adsorption capacity of ZIF-8 samples toward toluene was measured using breakthrough curves obtained under different experimental conditions. The breakthrough curves are the concentration-time profile, which are expressed in term of C/C_0 as a function of time (where C is effluent and C_0 is influent concentration of the toluene). A known concentration of toluene was passed through the fixed bed of the adsorbent, and the concentration of toluene at effluent of the reactor was measured. The concentration of toluene in the feed was controlled at 1000 ppmv by using a $0.02 \text{ L} \cdot \text{min}^{-1}$ flow rate of the carrier gas (Q). The amount of adsorbent (M) in each experiment was 0.05 g, which was packed into the quartz tube. The time of the breakthrough adsorption t_b (min) and time of the equilibrium adsorption t_e (min) were determined, while the ratio of influent and effluent toluene concentrations (C/C_0) were equal to 0.05 and 0.95, respectively. Breakthrough capacity was measured using the following equation [24,42,43]:

$$q = \frac{QC_0}{M} t_e - \frac{Q}{M} \int_0^{t_e} C \cdot dt_e \quad (1)$$

where q is the breakthrough capacity ($\text{mg} \cdot \text{g}^{-1}$), which is indeed the total mass of toluene adsorbed on ZIF-8 (M). In Equation (1) the first term is the total toluene in the influent gas relative to the mass of ZIF-8 in the duration of t_e and the second term is the total mass of toluene in the effluent gas.

The total adsorption percentage of toluene (A) was calculated using the following equation [44]:

$$A = \frac{s}{x} \times 100 \quad (2)$$

where s is the adsorbed toluene (mg) on ZIF-8 and x is the total amount of toluene in influent (mg) in the duration of t_e .

2.5. Activation of ZIF-8

The adsorption performances of ZIF-8 were examined after pretreatment of adsorbents in various conditions and the results were compared with the performances of the as-synthesized ZIF-8. Pretreatment processes were performed in dry air and N_2 atmospheres. In each process 0.05 g of ZIF-8 was packed into the quartz tube and heated to anticipated temperatures under nitrogen or dried air at a flow rate of $0.02 \text{ L} \cdot \text{min}^{-1}$ for 180 min. The adsorbents were heated in dry air at 300°C , while the N_2 atmosphere was pretreated at 300°C and 400°C . Activated ZIF-8 samples were cooled to ambient temperature, then adsorption tests were carried out. The activation temperatures were selected based on the results of previous studies on ZIF-8's thermal stability [31,36,37,45].

2.6. The Effect of RH

The effect of relative humidity (RH) on adsorption capacity, total adsorption percentage, time of breakthrough, and time of equilibration of toluene adsorption on ZIF-8 were studied. All samples were pretreated in the optimal condition.

The flow rate of carrier gas was set at $0.02 \text{ L} \cdot \text{min}^{-1}$ by mass flow controller (MFC). The temperature of the silicon oil bath that contained a distilled water flask was adjusted so that the desired RH (40%, 60% and 80%) was achieved in the influent gas. A constant concentration of toluene (1000 ppmv) was achieved by adjusting the rate of toluene injection by a syringe pump. GC-FID analysis was used to check the toluene concentration.

3. Results and Discussion

3.1. Characterization

The XRD pattern of as-synthesized ZIF-8 is shown in Figure 1a. This pattern is similar to the XRD pattern simulated by Park and et al. [31]. Characteristic peaks at 2θ of 7.35° , 10.40° , 12.75° , 14.73° , 16.48° , 22.18° and 24.55° ascertain the formation of a high-purity crystalline phase ZIF-8.

Figure 1b shows the FT-IR spectra of as-synthesized ZIF-8 which is in very good agreement with previously-reported FT-IR bands of ZIF-8 [32,38,39,46]. The adsorption bands for ZIF-8 at 3135 and 2929 cm^{-1} can be assigned to the aromatic and aliphatic C-H stretch of imidazole, respectively. The band at 1584 cm^{-1} belongs to the C=N stretch and the peak at 1606 cm^{-1} can be assigned to the C=C stretch. The 421 cm^{-1} band is for Zn-N stretching mode. In addition, the peaks in the region of $1350\text{--}1500\text{ cm}^{-1}$ belong to the entire ring stretching. The in-plane bending of the ring are found in the $900\text{--}1350\text{ cm}^{-1}$ while those below 800 cm^{-1} are associated with the out-of-plane bending of the ring.

The morphologies and particle size distributions of as-synthesized ZIF-8 were studied using SEM imagery, which are depicted in Figure 1c,d, respectively. The cubic shape of the ZIF-8 crystals can be seen from SEM image clearly. The mean and standard deviation of the particle sizes of ZIF-8 is ca. $0.64\text{ }\mu\text{m}$ and 0.08 , respectively.

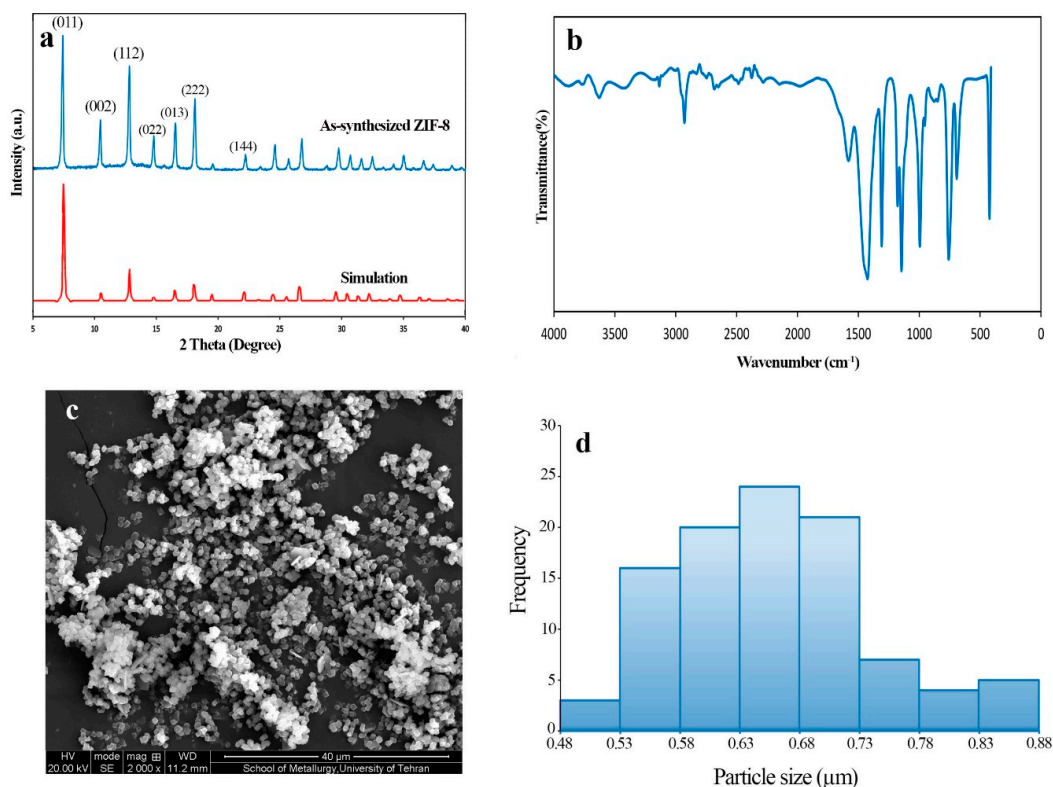


Figure 1. (a) XRD and simulated pattern of the Zeolitic imidazolate framework-8 (ZIF-8); (b) fourier transform infrared (FT-IR) spectra of the ZIF-8; (c) SEM micrograph of the as-synthesized ZIF-8 at magnification of 2000; and (d) distribution histogram of the particle size calculated from the SEM image.

3.2. Effects of Thermal Activation

Breakthrough curves of toluene adsorption on the as-synthesized and activated ZIF-8 samples (in the dry air and N_2 atmospheres) are shown in Figure 2a,b. The breakthrough curve fluctuated slightly, which is due to the dynamics of the process. For air-activation, the process was carried out for 3 h at 300°C under constant flow of dry air (labeled as ZIF-8/Air/ 300°C). N_2 activation, however, was performed at 300°C or 400°C (labeled as ZIF-8/ N_2 / 300°C and ZIF-8/ N_2 / 400°C).

The flow rate of the influent gas (dry air or N₂) was controlled at 0.02 L·min⁻¹. After the activation process, adsorption performances of 0.05 g of each ZIF-8 sample was studied at 1000 ppmv of toluene concentration under a carrier gas flow rate of 0.02 L·min⁻¹ at the desired temperature (e.g., 300 °C or 400 °C).

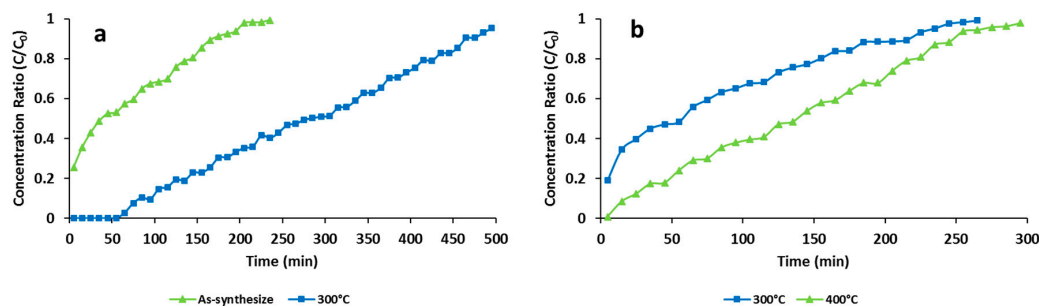


Figure 2. Breakthrough curves of toluene adsorption at zero relative humidity (RH) on (a) as-synthesized ZIF-8 and ZIF-8 activated at 300 °C in the air flow (ZIF-8/Air/300 °C) and (b) ZIF-8 activated at 300 °C (ZIF-8/N₂/300 °C) and 400 °C (ZIF-8/N₂/400 °C) in N₂ flow.

The adsorption parameters such as, breakthrough point, time of equilibration, adsorption capacity, and total adsorption percentage of the tested ZIF-8 adsorbents are summarized in Table 1. It can be seen that activation of the synthesized ZIF-8 improved its adsorption efficiency for capturing toluene. The ZIF-8/Air/300 °C sample showed a significantly higher breakthrough point, equilibration time, adsorption capacity, and total adsorption percent compared to the other samples. Chu et al. investigated toluene adsorption by ZIF-8/graphene oxide (GO) hybrid composite with different proportions of GO. They reported that toluene adsorption capacity of ZIF-8/GO with a GO content of 4 wt % was equal to 116 mg·g⁻¹ [47]. Bahri et al. studied the breakthrough behaviors of three MOF, MIL-101, MIL-53, and CPM-5 for toluene whose adsorption capacity was equal to 211.5, 73, and 38.8 mg·g⁻¹ respectively [24].

Table 1. The effects of different pretreatment conditions on the operational parameters of toluene adsorption on Zeolitic imidazolate framework-8 (ZIF-8).

Pretreatment Condition	Adsorption Capacity (mg·g ⁻¹)	Total Adsorption Percentage (%)	Time of Breakthrough (min)	Time of Equilibration (min)
As-synthesized	131.43	26.84	0	205
ZIF-8/Air/300 °C	562.17	55.66	65	495
ZIF-8/N ₂ /300 °C	155.31	27.48	0	265
ZIF-8/N ₂ /400 °C	260.87	43.95	10	295

Adsorption efficiency of the ZIF-8/N₂/400 °C sample was lower than the ZIF-8/Air/300 °C and higher than the ZIF-8/N₂/300 °C sample. This reveals that N₂ activation temperature is temperature-dependent. It has been reported that thermal activation of ZIF-8 under an inert gas atmosphere (e.g., nitrogen) helps to remove guest molecules that are attached to the surface of samples [36], however, it cannot remove unreacted linkers and guest molecules that are trapped during the course of the synthesis process in pores and cavities of the crystalline sample [32]. This can explain the lower adsorption efficiency of the ZIF-8 samples activated under N₂ atmosphere.

On the other hand, however, activating ZIF-8 adsorbents under a dry air atmosphere at high temperature (i.e., 300 °C) provides a strong oxidizing condition for decomposing molecules trapped in the cavities and pores of ZIF-8. Therefore, dry air activation of ZIF-8 makes more adsorption sites accessible to toluene molecules, resulting in an improved adsorption performance of the activated adsorbent.

XRD patterns of the ZIF-8 after activation at different conditions are illustrated in Figure 3a. The XRD patterns reveal that ZIF-8 structure remained intact after activation. The difference in peak intensity can be attributed to variations in the scattering intensity of the components of the crystal structure and their arrangement in the lattice. Some of the changes can be related to interference between diffractions.

FT-IR spectra of the ZIF-8/Air/300, ZIF-8/N₂/400, and as-synthesized ZIF-8 are shown in Figure 3b. It can be seen that FT-IR bands assigned to the ZIF-8 structure are similar in all samples.

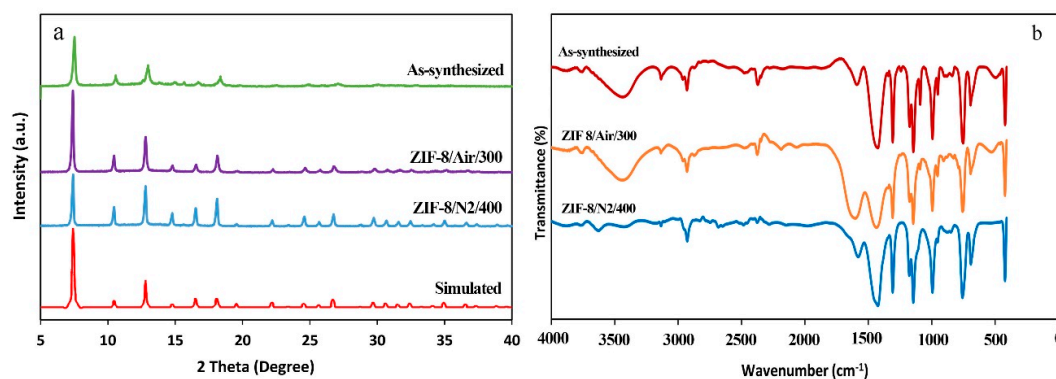


Figure 3. (a) XRD pattern and (b) FT-IR spectra of ZIF-8 after activation at different conditions.

Previous studies confirmed that thermal stability of ZIF-8 depends on the temperature, atmosphere, and exposure time [31,36,37]. It is reported that ZIF-8 was stable under dry air atmosphere up to 300 °C for 5 h, however it was unstable at the same temperature (i.e., 300 °C) after 24 h of heat treatment. Furthermore, the ZIF-8 structure collapsed after heat treatment under dry air at 400 °C for 5 h [37]. Thermal gravimetric analysis (TGA) of ZIF-8 under N₂ atmosphere indicated that the structure could tolerate temperatures as high as 550 °C [31].

3.3. The Effects of RH on Toluene Adsorption

The effects of RH of 40%, 60% and 80% on the adsorption of toluene was studied on 0.05 g of the ZIF-8/Air/300 °C adsorbent at 25 °C with a constant feed (toluene) concentration of 1000 ppmv in N₂ (as the carrier gas). The breakthrough curves of toluene adsorption on ZIF-8/Air/300 °C sample at RH of 40%, 60% and 80% are depicted in Figure 4.

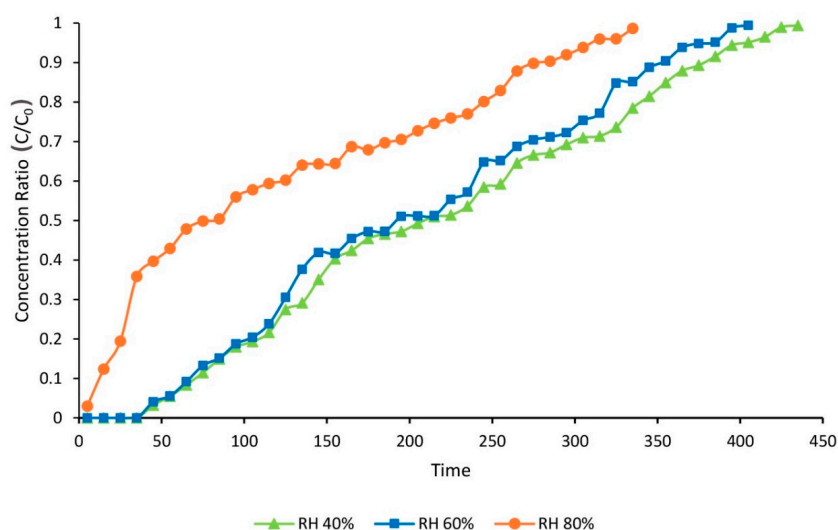


Figure 4. Breakthrough curves of toluene adsorption on ZIF-8/Air/300 °C at 40%, 60%, and 80% RH.

Different adsorption parameters such as breakthrough point, equilibration time, adsorption capacity, and total adsorption percentage for the adsorbent examined at different RH are summarized in Table 2. While increasing of RH from 40% to 60% did not affect the breakthrough point (e.g., 55 min), however slightly decreased the saturation pint resulting in slight reduction of adsorption capacity (i.e., from ~411 to 359 mg·g⁻¹). Further increasing of RH of feed stream to 80% resulted in substantial shortening of breakthrough point to 5 min and adsorption capacity to 230 mg·g⁻¹ (Table 2).

Table 2. The effects of different relative humidity on the operational parameters of toluene adsorption on ZIF-8.

Relative Humidity (%)	Adsorption Capacity (mg·g ⁻¹)	Total Adsorption Percentage (%)	Time of Breakthrough (min)	Time of Equilibration (min)
40	410.9	48.8	55	435
60	354	48.9	55	405
80	203.3	33.8	5	335

In general, MOFs structure has an amphiphilic property, in which metal clusters are hydrophilic and organic linkers are lipophilic [24,48]. Both metal sites and linkers (e.g., functional groups) act as adsorption site in MOFs structure [24]. In the ZIF-8 structure, H₂O molecules are adsorbed by Zn(II) sites (hydrophilic sites) and toluene molecules are adsorbed by 2-methylimidazol linkers (lipophilic sites). Although the Zn(II) coordinates are saturated with imidazole, however, some of Zn(II) ions are not completely coordinated with the linker during the ZIF-8 synthesis. This structural defects form open metal sites (defect sites) can act as water adsorption sites [49]. In addition, at higher RH, water adsorption can be increased because of capillary condensation [50]. The decreasing trend of toluene adsorption by increasing the RH from 40% to 60% and 80% can be attributed to the hydrophilic characteristics of metal sites in ZIF-8 structure.

FT-IR spectra of the toluene saturated ZIF-8/Air/300 °C (i.e., after toluene adsorption at different RH) are illustrated in Figure 5a–c. Comparing these spectra with those of fresh adsorbent (Figure 5b) reveals that the adsorption bands at 3034 cm⁻¹ can be assigned as the =C–H stretch of the toluene aromatic ring. The band at 2925 cm⁻¹ is for –C–H stretch of methylene group and the peaks at 1614 cm⁻¹, 1506 cm⁻¹, and 1450 cm⁻¹ belong to the C=C aromatic ring stretching [51].

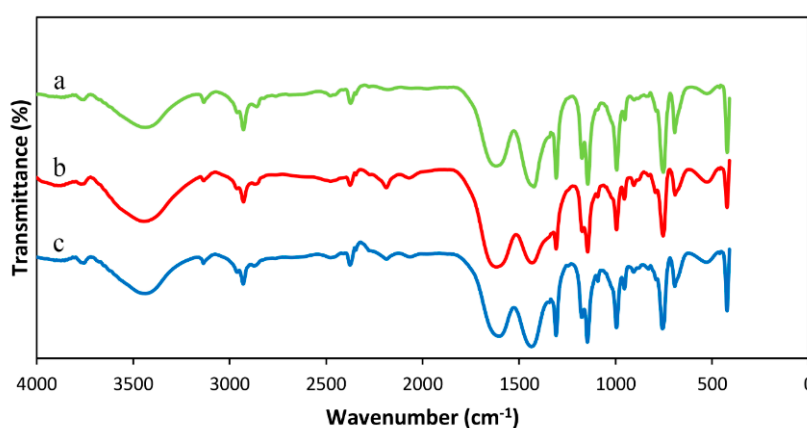


Figure 5. FT-IR spectra of ZIF-8/Air/300 °C after toluene adsorption at (a) 40% RH; (b) 60% RH; and (c) 80% RH.

3.4. Mathematical Modeling

Mathematical modeling and simulation is a very useful tool to predict the adsorption/desorption process in a fixed bed column [52].

For successful design of a continuous adsorption system, the prediction of the breakthrough curve is very crucial. Maximum adsorption capacity of the adsorbent is another important parameter that is needed for a reactor design. Experimental data and mathematical modeling are used to obtain breakthrough curves of a desired adsorption system. In comparison with experimental method, mathematical modeling is simple, economic, and quick. Thus, they are used increasingly by researchers [53].

In this study, the experimental breakthrough curves were fitted with Yan and Thomas models to predict adsorption parameters. Equations (3) and (4) describe the Yan and Thomas models, respectively [52,53]:

$$\frac{C}{C_0} = 1 - \frac{1}{1 + \left(\frac{C_0 Q}{q_y m} t\right)^{A_y}} \quad (3)$$

$$\frac{C}{C_0} = \frac{1}{1 + \exp\left(\frac{K_T q_T m}{Q} - K_T C_0 t\right)} \quad (4)$$

where A_y is the Yan models' constant and K_T is the Thomas models' constant. q_y and q_T denote adsorption capacity of the adsorbents, which can be estimated by Yan and Thomas models ($\text{mg} \cdot \text{g}^{-1}$). In the current work A_y , K_T , q_y , and q_T parameters were estimated by fitting the collected experimental data into the Equations (3) and (4).

Statistical parameters of fitting such as squared correlation coefficient (R^2), adjusted squared correlation coefficient (R^2_{adj}), root mean square error (RMSE), and sum square error (SSE) were computed in order to evaluate the characteristics of fitting models. The Trust-Region algorithm was used to perform non-linear least square fitting of the adsorption parameters using MATLAB software (Mathwork Inc., Natick, MA, USA).

The Yan and Thomas mathematical models [52,53] were used to fit the experimental breakthrough curves using non-linear curve fitting (Figures 6–8). Statistical parameters of the fitting are summarized in the Table 3.

In case of adsorption by ZIF-8/Air/300 °C (Figure 6a), the values of R^2_{adj} and R^2 in the Yan and Thomas models was 0.98, with low values of RMSE and SSE in both models (Table 3), which indicate good fitness of the experimental data with the mathematical models. In addition, the values of q_y and q_T that are estimated by the Yan and Thomas models, respectively, are very close to the values obtained from the experimental data (Table 3).

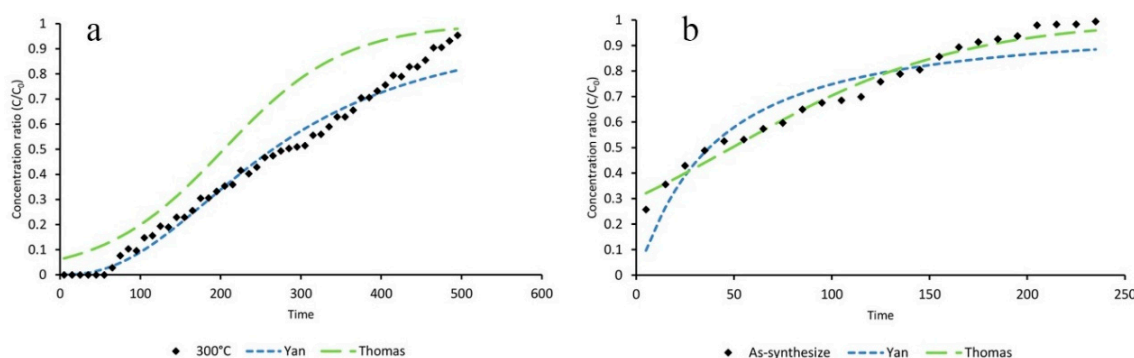


Figure 6. Experimental and predicted breakthrough curves of toluene adsorbed on (a) ZIF-8/Air/300 °C and (b) as-synthesized ZIF-8.

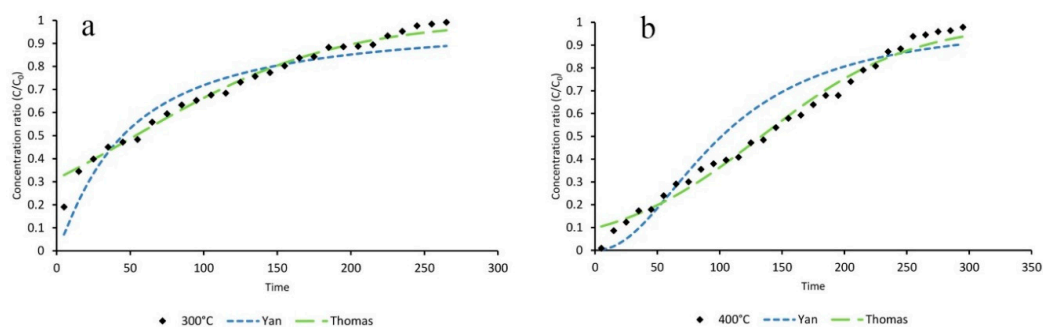


Figure 7. Experimental and predicted breakthrough curves of toluene adsorbed on (a) ZIF-8/N₂/300 °C and (b) ZIF-8/N₂/400 °C.

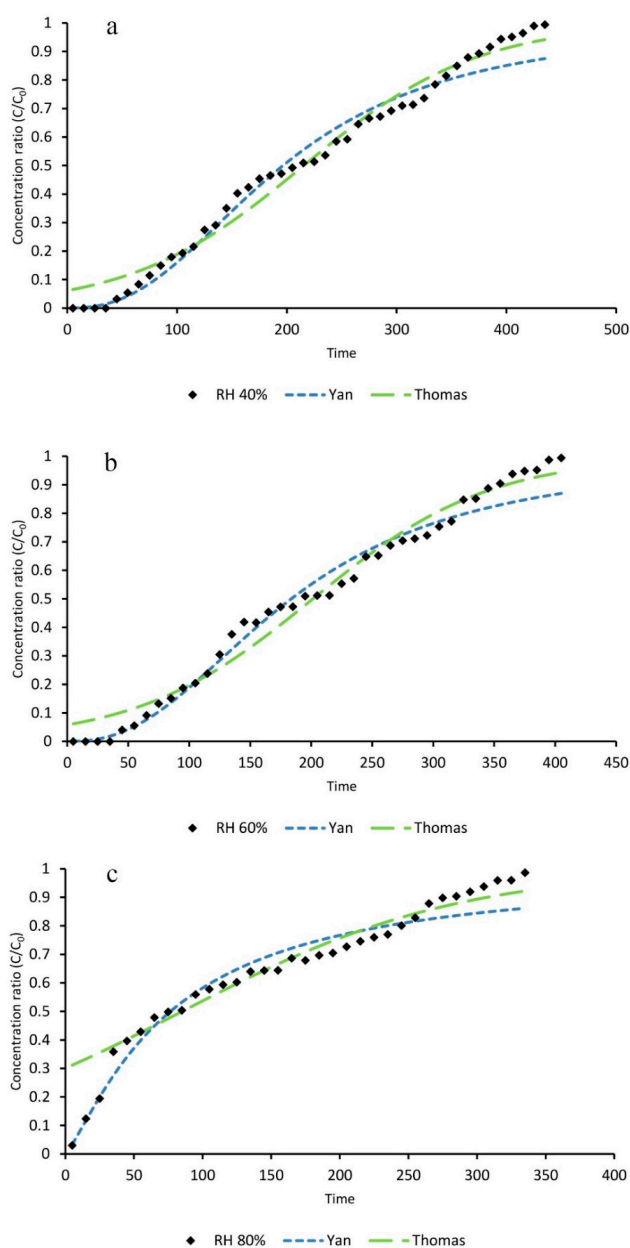


Figure 8. Experimental and predicted breakthrough curves of toluene adsorption on ZIF-8/Air/300 °C at relative humidity (a) 40%; (b) 60%; and (c) 80%.

The experimental and simulated breakthrough curves of toluene adsorption on ZIF-8/N₂/300 °C and ZIF-8/N₂/400 °C samples are shown in Figure 7a,b. The calculated parameters are listed in Table 3. The results indicate that the Thomas model offers a better fit for the experimental breakthrough data compared to the Yan model. Furthermore, the adsorption capacity estimated by the Thomas model (q_T) was closer to the values calculated from the experimental data (Table 4).

Table 3. Statistical parameters obtained from the fitting of toluene breakthrough curves of ZIF-8 (activated in the different conditions) using the Yan and Thomas models. RMSE: root mean square error; SSE: sum square error.

Statistical Parameters		As-Synthesized	ZIF-8/Air/300 °C	ZIF-8/N ₂ /300 °C	ZIF-8/N ₂ /400 °C
Thomas	K_T	3.26	1.98	2.75	3.33
	R^2	0.97	0.98	0.99	0.98
	R^2_{adj}	0.97	0.98	0.99	0.98
	RMSE	0.034	0.043	0.022	0.038
	SSE	0.026	0.88	0.012	0.04
Yan	A_y	1.11	2.37	1.17	2.1
	R^2	0.84	0.98	0.89	0.93
	R^2_{adj}	0.84	0.98	0.89	0.93
	RMSE	0.086	0.044	0.071	0.077
	SSE	0.16	0.095	0.13	0.16

Table 4. Estimated adsorption capacity of ZIF-8 (activated in the different conditions) by the Yan and Thomas models and comparison with the experimental data.

Adsorption Capacity	As-Synthesize (mg·g ⁻¹)	ZIF-8/Air/300 °C (mg·g ⁻¹)	ZIF-8/N ₂ /300 °C (mg·g ⁻¹)	ZIF-8/N ₂ /400 °C (mg·g ⁻¹)
q_T (Thomas)	102.3	578.2	114.4	268.3
q_y (Yan)	78.1	540.8	95.72	204
q (Experimental)	131.43	562.17	155.31	260.87

Figure 8a–c shows the simulated breakthrough curves resulted from the fitting of experimental data in the Yan and Thomas models. The statistical parameters and the estimated adsorption capacity of the modeling are represented in Tables 5 and 6, respectively. Results of mathematical modeling revealed that the breakthrough curves of the toluene adsorption at all tested RH fit very well with the Thomas model. The Yan model, however, predicts the breakthrough curves at RH of 40% and 60% are more accurate compared to those of RH of 80%.

Table 5. Statistical parameters obtained from the fitting of toluene breakthrough curves of ZIF-8 (adsorption at 40%, 60%, and 80% RH) using the Yan and Thomas models.

Statistical Parameters		Relative Humidity (%)		
		40	60	80
Thomas	K_T	2.62	3.1	2.21
	R^2	0.97	0.97	0.97
	R^2_{adj}	0.97	0.97	0.97
	RMSE	0.052	0.054	0.041
	SSE	0.11	0.11	0.055
Yan	A_y	2.45	2.4	1.24
	R^2	0.97	0.97	0.94
	R^2_{adj}	0.97	0.97	0.94
	RMSE	0.053	0.054	0.06
	SSE	0.12	0.12	0.11

Table 6. Estimated adsorption capacity of ZIF-8 (adsorption at 40%, 60%, and 80% RH) by the Yan and Thomas models and comparison with the experimental data.

Adsorption Capacity	Relative Humidity (%)		
	40	60	80
q_T (Thomas)	416.3	360.1	152.6
q_Y (Yan)	379.7	328.4	137.2
q (Experimental)	410	354	203.3

By looking at the breakthrough curves (Figures 6–8) and the statistical parameters (Tables 3–6) it can be concluded that the Yan equation (compared to the Thomas equation) is more suitable for accurate simulation of breakthrough curves with sigmoidal or tilted S shapes. This finding is in accordance with other studies [52].

4. Conclusions

ZIF-8 was synthesized from aqueous solution, and should be considered as a facile and environmentally-friendly method. Adsorption of toluene by the ZIF-8 and its activated form was examined in a continuous mode using a fixed bed reactor. Adsorption parameters were calculated from the obtained breakthrough curves. The results of thermal activation under dry air and N_2 atmospheres revealed that an oxidizing condition would result a ZIF-8 adsorbent with higher adsorption capacity for capturing toluene from polluted air streams. ZIF-8 activated under dry airflow at 300 °C for 3 h proved to be the most efficient adsorbent for toluene under the tested conditions.

Experimental data of the dynamic adsorption of toluene showed that toluene removal efficiencies of activated ZIF-8 did not change significantly by increasing the RH from 40% to 60%. However, its adsorption capacity dropped dramatically at RH higher than 80%. It can be concluded that activated ZIF-8 should be considered an efficient adsorbent for toluene removal at low and medium RH (e.g., 40–60%).

The breakthrough curve of toluene adsorption on activated ZIF-8 under different conditions were simulated by fitting the experimental data into the Yan and Thomas mathematical models. The statistical parameters, such as root mean square error (RMSE), sum square error (SSE), squared correlation coefficient (R^2), and adjusted squared correlation coefficient (R^2_{adj}), were calculated and evaluated. It was concluded that both models could be applicable for curve fitting of toluene dynamic adsorption on activated ZIF-8 at different RH.

Acknowledgments: The authors would like to thank Hamadan University of Medical Sciences for the financial support under PhD thesis scheme (number: 9312126593).

Author Contributions: Saeed Jafari, Farshid Ghorbani-Shahna, Abdulrahman Bahrami, and Hossein Kazemian conceived and designed the experiments; Saeed Jafari performed the experiments; Saeed Jafari and Farshid Ghorbani-Shahna analyzed the data; Saeed Jafari contributed reagents/materials/analysis tools; Saeed Jafari, Farshid Ghorbani-Shahna, Abdulrahman Bahrami, and Hossein Kazemian wrote the paper.

Conflicts of Interest: The authors state that they have no conflict of interest.

References

1. Cetin, E.; Odabasi, M.; Seyfioglu, R. Ambient volatile organic compound (voc) concentrations around a petrochemical complex and a petroleum refinery. *Sci. Total Environ.* **2003**, *312*, 103–112. [[CrossRef](#)]
2. Hu, Q.; Li, J.J.; Hao, Z.P.; Li, L.D.; Qiao, S.Z. Dynamic adsorption of volatile organic compounds on organofunctionalized sba-15 materials. *Chem. Eng. J.* **2009**, *149*, 281–288. [[CrossRef](#)]
3. Mohan, N.; Kannan, G.K.; Upendra, S.; Subha, R.; Kumar, N.S. Breakthrough of toluene vapours in granular activated carbon filled packed bed reactor. *J. Hazard. Mater.* **2009**, *168*, 777–781. [[CrossRef](#)] [[PubMed](#)]
4. Liotta, L.F. Catalytic oxidation of volatile organic compounds on supported noble metals. *Appl. Catal. B* **2010**, *100*, 403–412. [[CrossRef](#)]

5. Feron, V.J.; Til, H.P.; de Vrijer, F.; Van Bladeren, P.J. Toxicology of volatile organic compounds in indoor air and strategy for further research. *Indoor Environ.* **1992**, *1*, 1016–4901. [[CrossRef](#)]
6. Zhang, X.; Gao, B.; Creamer, A.E.; Cao, C.; Li, Y. Adsorption of vocs onto engineered carbon materials: A review. *J. Hazard. Mater.* **2017**, *338*, 102–123. [[CrossRef](#)] [[PubMed](#)]
7. Wang, S.; Ang, H.M.; Tade, M.O. Volatile organic compounds in indoor environment and photocatalytic oxidation: State of the art. *Environ. Int.* **2007**, *33*, 694–705. [[CrossRef](#)] [[PubMed](#)]
8. Li, L.; Wang, S.B.; Feng, Q.C.; Liu, J.X. Removal of o-xylene from off-gas by a combination of bioreactor and adsorption. *Asia-Pac. J. Chem. Eng.* **2008**, *3*, 489–496. [[CrossRef](#)]
9. Shahna, F.G.; Golbabaie, F.; Hamed, J.; Mahjub, H.; Darabi, H.R.; Shahtaheri, S.J. Treatment of benzene, toluene and xylene contaminated air in a bioactive foam emulsion reactor. *Chin. J. Chem. Eng.* **2010**, *18*, 113–121. [[CrossRef](#)]
10. Brosillon, S.; Manero, M.-H.; Foussard, J.-N. Mass transfer in voc adsorption on zeolite: Experimental and theoretical breakthrough curves. *Environ. Sci. Technol.* **2001**, *35*, 3571–3575. [[CrossRef](#)] [[PubMed](#)]
11. Wang, S.; Zhang, L.; Long, C.; Li, A. Enhanced adsorption and desorption of vocs vapor on novel micro-mesoporous polymeric adsorbents. *J. Colloid Interface Sci.* **2014**, *428*, 185–190. [[CrossRef](#)] [[PubMed](#)]
12. Yu, W.; Yuan, P.; Liu, D.; Deng, L.; Yuan, W.; Tao, B.; Cheng, H.; Chen, F. Facile preparation of hierarchically porous diatomite/mfi-type zeolite composites and their performance of benzene adsorption: The effects of naoh etching pretreatment. *J. Hazard. Mater.* **2015**, *285*, 173–181. [[CrossRef](#)] [[PubMed](#)]
13. Qiang, Z.; Guo, Y.; Liu, H.; Cheng, S.Z.D.; Cakmak, M.; Cavicchi, K.A.; Vogt, B.D. Large-scale roll-to-roll fabrication of ordered mesoporous materials using resol-assisted cooperative assembly. *ACS Appl. Mater. Interfaces* **2015**, *7*, 4306–4310. [[CrossRef](#)] [[PubMed](#)]
14. Qiang, Z.; Gurkan, B.; Ma, J.; Liu, X.; Guo, Y.; Cakmak, M.; Cavicchi, K.A.; Vogt, B.D. Roll-to-roll fabrication of high surface area mesoporous carbon with process-tunable pore texture for optimization of adsorption capacity of bulky organic dyes. *Microporous Mesoporous Mater.* **2016**, *227*, 57–64. [[CrossRef](#)]
15. Brauer, H.; Varma, Y.B.G. *Air Pollution Control Equipment*; Springer Science & Business Media: Berlin/Heidelberg, Germany, 2012.
16. Ma, F.-J.; Liu, S.-X.; Liang, D.-D.; Ren, G.-J.; Wei, F.; Chen, Y.-G.; Su, Z.-M. Adsorption of volatile organic compounds in porous metal-organic frameworks functionalized by polyoxometalates. *J. Solid State Chem.* **2011**, *184*, 3034–3039. [[CrossRef](#)]
17. Kosuge, K.; Kubo, S.; Kikukawa, N.; Takemori, M. Effect of pore structure in mesoporous silicas on voc dynamic adsorption/desorption performance. *Langmuir* **2007**, *23*, 3095–3102. [[CrossRef](#)] [[PubMed](#)]
18. Britt, D.; Tranchemontagne, D.; Yaghi, O.M. Metal-organic frameworks with high capacity and selectivity for harmful gases. *Proc. Natl. Acad. Sci. USA* **2008**, *105*, 11623–11627. [[CrossRef](#)] [[PubMed](#)]
19. Luebbers, M.T.; Wu, T.; Shen, L.; Masel, R.I. Trends in the adsorption of volatile organic compounds in a large-pore metal-organic framework, irmo-1. *Langmuir* **2010**, *26*, 11319–11329. [[CrossRef](#)] [[PubMed](#)]
20. Hasan, Z.; Jhung, S.H. Removal of hazardous organics from water using metal-organic frameworks (mofs): Plausible mechanisms for selective adsorptions. *J. Hazard. Mater.* **2015**, *283*, 329–339. [[CrossRef](#)] [[PubMed](#)]
21. Sabouni, R.; Kazemian, H.; Rohani, S. Carbon dioxide adsorption in microwave-synthesized metal organic framework cpm-5: Equilibrium and kinetics study. *Microporous Mesoporous Mater.* **2013**, *175*, 85–91. [[CrossRef](#)]
22. Sabouni, R.; Kazemian, H.; Rohani, S. Mathematical modeling and experimental breakthrough curves of carbon dioxide adsorption on metal organic framework cpm-5. *Environ. Sci. Technol.* **2013**, *47*, 9372–9380. [[CrossRef](#)] [[PubMed](#)]
23. Bahri, M.; Haghighat, F.; Rohani, S.; Kazemian, H. Metal organic frameworks for gas-phase vocs removal in a ntp-catalytic reactor. *Chem. Eng. J.* **2017**, *320*, 308–318. [[CrossRef](#)]
24. Bahri, M.; Haghighat, F.; Kazemian, H.; Rohani, S. A comparative study on metal organic frameworks for indoor environment application: Adsorption evaluation. *Chem. Eng. J.* **2017**, *313*, 711–723. [[CrossRef](#)]
25. Kumar, P.; Kim, K.-H.; Kwon, E.E.; Szulejko, J.E. Metal-organic frameworks for the control and management of air quality: Advances and future direction. *J. Mater. Chem. A* **2016**, *4*, 345–361. [[CrossRef](#)]
26. Gordon, J.; Kazemian, H.; Rohani, S. Mil-53(fe), mil-101, and sba-15 porous materials: Potential platforms for drug delivery. *Mater. Sci. Eng. C Mater. Biol. Appl.* **2015**, *47*, 172–179. [[CrossRef](#)] [[PubMed](#)]

27. Stassen, I.; Burtch, N.; Talin, A.; Falcaro, P.; Allendorf, M.; Ameloot, R. An updated roadmap for the integration of metal-organic frameworks with electronic devices and chemical sensors. *Chem. Soc. Rev.* **2017**, *46*, 3185–3241. [[CrossRef](#)] [[PubMed](#)]
28. Chen, Y.-M.; Liang, W.; Li, S.; Zou, F.; Bhaway, S.M.; Qiang, Z.; Gao, M.; Vogt, B.D.; Zhu, Y. A nitrogen doped carbonized metal-organic framework for high stability room temperature sodium-sulfur batteries. *J. Mater. Chem. A* **2016**, *4*, 12471–12478. [[CrossRef](#)]
29. Wang, J.-W.; Li, N.-X.; Li, Z.-R.; Wang, J.-R.; Xu, X.; Chen, C.-S. Preparation and gas separation properties of zeolitic imidazolate frameworks-8 (zif-8) membranes supported on silicon nitride ceramic hollow fibers. *Ceram. Int.* **2016**, *42*, 8949–8954. [[CrossRef](#)]
30. Venna, S.R.; Carreon, M.A. Highly permeable zeolite imidazolate framework-8 membranes for co₂/ch₄ separation. *J. Am. Chem. Soc.* **2009**, *132*, 76–78. [[CrossRef](#)] [[PubMed](#)]
31. Park, K.S.; Ni, Z.; Cote, A.P.; Choi, J.Y.; Huang, R.; Uribe-Romo, F.J.; Chae, H.K.; O’Keeffe, M.; Yaghi, O.M. Exceptional chemical and thermal stability of zeolitic imidazolate frameworks. *Proc. Natl. Acad. Sci. USA* **2006**, *103*, 10186–10191. [[CrossRef](#)] [[PubMed](#)]
32. He, M.; Yao, J.; Liu, Q.; Wang, K.; Chen, F.; Wang, H. Facile synthesis of zeolitic imidazolate framework-8 from a concentrated aqueous solution. *Microporous Mesoporous Mater.* **2014**, *184*, 55–60. [[CrossRef](#)]
33. Sava, D.F.; Rodriguez, M.A.; Chapman, K.W.; Chupas, P.J.; Greathouse, J.A.; Crozier, P.S.; Nenoff, T.M. Capture of volatile iodine, a gaseous fission product, by zeolitic imidazolate framework-8. *J. Am. Chem. Soc.* **2011**, *133*, 12398–12401. [[CrossRef](#)] [[PubMed](#)]
34. Tsai, C.-W.; Langner, E.H.G. The effect of synthesis temperature on the particle size of nano-zif-8. *Microporous Mesoporous Mater.* **2016**, *221*, 8–13. [[CrossRef](#)]
35. Ania, C.O.; Garcia-Perez, E.; Haro, M.; Gutierrez-Sevillano, J.J.; Valdes-Solis, T.; Parra, J.B.; Calero, S. Understanding gas-induced structural deformation of zif-8. *J. Phys. Chem. Lett.* **2012**, *3*, 1159–1164. [[CrossRef](#)] [[PubMed](#)]
36. Pan, Y.; Liu, Y.; Zeng, G.; Zhao, L.; Lai, Z. Rapid synthesis of zeolitic imidazolate framework-8 (zif-8) nanocrystals in an aqueous system. *Chem. Commun.* **2011**, *47*, 2071–2073. [[CrossRef](#)] [[PubMed](#)]
37. Yin, H.; Kim, H.; Choi, J.; Yip, A.C.K. Thermal stability of zif-8 under oxidative and inert environments: A practical perspective on using zif-8 as a catalyst support. *Chem. Eng. J.* **2015**, *278*, 293–300. [[CrossRef](#)]
38. Hu, Y.; Kazemian, H.; Rohani, S.; Huang, Y.; Song, Y. In situ high pressure study of zif-8 by ftir spectroscopy. *Chem. Commun.* **2011**, *47*, 12694–12696. [[CrossRef](#)] [[PubMed](#)]
39. Cravillon, J.; Munzer, S.; Lohmeier, S.-J.; Feldhoff, A.; Huber, K.; Wiebcke, M. Rapid room-temperature synthesis and characterization of nanocrystals of a prototypical zeolitic imidazolate framework. *Chem. Mater.* **2009**, *21*, 1410–1412. [[CrossRef](#)]
40. Bustamante, E.L.; Fernandez, J.L.; Zamaro, J.M. Influence of the solvent in the synthesis of zeolitic imidazolate framework-8 (zif-8) nanocrystals at room temperature. *J. Colloid. Interface. Sci.* **2014**, *424*, 37–43. [[CrossRef](#)] [[PubMed](#)]
41. Bao, Q.; Lou, Y.; Xing, T.; Chen, J. Rapid synthesis of zeolitic imidazolate framework-8 (zif-8) in aqueous solution via microwave irradiation. *Inorg. Chem. Commun.* **2013**, *37*, 170–173. [[CrossRef](#)]
42. Kim, K.-J.; Ahn, H.-G. The adsorption and desorption characteristics of a binary component system of toluene and methylethylketone on activated carbon modified with phosphoric acid. *Carbon* **2010**, *48*, 2198–2202. [[CrossRef](#)]
43. Liu, H.B.; Yang, B.; Xue, N.D. Enhanced adsorption of benzene vapor on granular activated carbon under humid conditions due to shifts in hydrophobicity and total micropore volume. *J. Hazard. Mater.* **2016**, *318*, 425–432. [[CrossRef](#)] [[PubMed](#)]
44. Zhang, J.; Zhang, X.L.; Li, H.; Zhao, B. Ion exchange adsorption studies of miglitol in a fixed bed. *Chem. Eng. Technol.* **2012**, *35*, 811–818. [[CrossRef](#)]
45. Jafari, S.; Ghorbani, F.; Bahrami, A.; Kazemian, H.; Yousefinejad, S. Removal of toluene from air by zeolitic imidazolate framework-8: Synthesis, characterization, and experimental breakthrough curve. *Int. J. Sci. Stud.* **2017**, *5*, 1073–1082. [[CrossRef](#)]
46. Ordoñez, M.J.C.; Balkus, K.J.; Ferraris, J.P.; Musselman, I.H. Molecular sieving realized with zif-8/matrimid®mixed-matrix membranes. *J. Membr. Sci.* **2010**, *361*, 28–37. [[CrossRef](#)]

47. Chu, F.; Zheng, Y.; Wen, B.; Zhou, L.; Yan, J.; Chen, Y. Adsorption of toluene with water on zeolitic imidazolate framework-8/graphene oxide hybrid nanocomposites in a humid atmosphere. *RSC Adv.* **2018**, *8*, 2426–2432. [[CrossRef](#)]
48. Zhao, Z.; Li, X.; Huang, S.; Xia, Q.; Li, Z. Adsorption and diffusion of benzene on chromium-based metal organic framework mil-101 synthesized by microwave irradiation. *Ind. Eng. Chem. Res.* **2011**, *50*, 2254–2261. [[CrossRef](#)]
49. Zhang, K.; Lively, R.P.; Zhang, C.; Koros, W.J.; Chance, R.R. Investigating the intrinsic ethanol/water separation capability of zif-8: An adsorption and diffusion study. *J. Phys. Chem. C* **2013**, *117*, 7214–7225. [[CrossRef](#)]
50. Küsgens, P.; Rose, M.; Senkovska, I.; Fröde, H.; Henschel, A.; Siegle, S.; Kaskel, S. Characterization of metal-organic frameworks by water adsorption. *Microporous Mesoporous Mater.* **2009**, *120*, 325–330. [[CrossRef](#)]
51. Serra, R.M.; Miró, E.E.; Boix, A.V. Ftir study of toluene adsorption on cs-exchanged mordenites. *Microporous Mesoporous Mater.* **2010**, *127*, 182–189. [[CrossRef](#)]
52. Yan, G.; Viraraghavan, T.; Chen, M. A new model for heavy metal removal in a biosorption column. *Adsorpt. Sci. Technol.* **2001**, *19*, 25–43. [[CrossRef](#)]
53. Xu, Z.; Cai, J.-G.; Pan, B.-C. Mathematically modeling fixed-bed adsorption in aqueous systems. *J. Zhejiang Univ. Sci. A* **2013**, *14*, 155–176. [[CrossRef](#)]



© 2018 by the authors. Licensee MDPI, Basel, Switzerland. This article is an open access article distributed under the terms and conditions of the Creative Commons Attribution (CC BY) license (<http://creativecommons.org/licenses/by/4.0/>).